Nature Methods

An artery-specific fluorescent dye for studying neurovascular coupling

Zhiming Shen, Zhongyang Lu, Pratik Y Chhatbar, Philip O'Herron & Prakash Kara

Supplementary Figure 1	Delay between the filling of arteries and veins after intravenous dye injection confirms artery specificity of Alexa 633 labeling *in vivo*
Supplementary Figure 2	Vessel classification using brightfield vs. two-photon fluorescein dextran + Alexa 633 *in vivo*
Supplementary Figure 3	Vessel classification using brightfield vs. two-photon green tomato lectin + Alexa 633 *in vivo*
Supplementary Figure 4	Persistent *in vivo* Alexa 633 labeling > 24 hours post-injection
Supplementary Figure 5	Surface and penetrating arterioles ≥ 15 μm in diameter are labeled *in vivo* by Alexa 633 while veins, venules, and microvessels are not
Supplementary Figure 6	The smallest surface arteriole branches (≤ 10 μm diameter) are not labeled by Alexa 633 *in vivo*
Supplementary Figure 7	A deep penetrating arteriole labeled by Alexa 633 *in vivo*
Supplementary Figure 8	Small (< 10-μm-diameter) branchlets off penetrating arterioles are not labeled by Alexa 633 *in vivo*
Supplementary Figure 9	PDGFR-β immunohistochemistry suggests that pericytes are not labeled by Alexa 633
Supplementary Figure 10	Alexa 633 does not label the small microvessels in histological sections of the cerebral cortex
Supplementary Figure 11	Arterioles but not venules in the visual cortex respond to drifting grating visual stimuli
Supplementary Figure 12	Neuronal responses are unaffected by local micropipette application of Alexa 633 in the visual cortex
Supplementary Figure 13	Neuronal responses are unaffected before and after intravenous application of Alexa 633 in the same animal
Supplementary Figure 14	EEG and heart rate are unaffected by Alexa 633

Supplementary Figure 15	Binding site of Alexa 633 on artery/arteriole wall
Supplementary Figure 16	Alexa 633 labels elastin fibers on artery walls in brain and aorta
Supplementary Figure 17	Alexa 633 labeling of human aorta
Supplementary Figure 18	Alexa 633 labeling of mouse kidney
Supplementary Figure 19	Red blood cell velocity in cortical microvessels after intravenous injection of fluorescent dyes
Supplementary Figure 20	Light path used for *in vivo* two-photon imaging
Supplementary Note 1	Fluorescence dip artifact caused by arteriole dilation
Supplementary Note 2	Selectivity of Alexa 633 vs. other rhodamine derivatives

Note: Supplementary Videos 1–4 are available on the Nature Methods website.

Supplementary Figure 1
Delay between the filling of arteries and veins after intravenous dye injection confirms artery specificity of Alexa 633 labeling *in vivo*

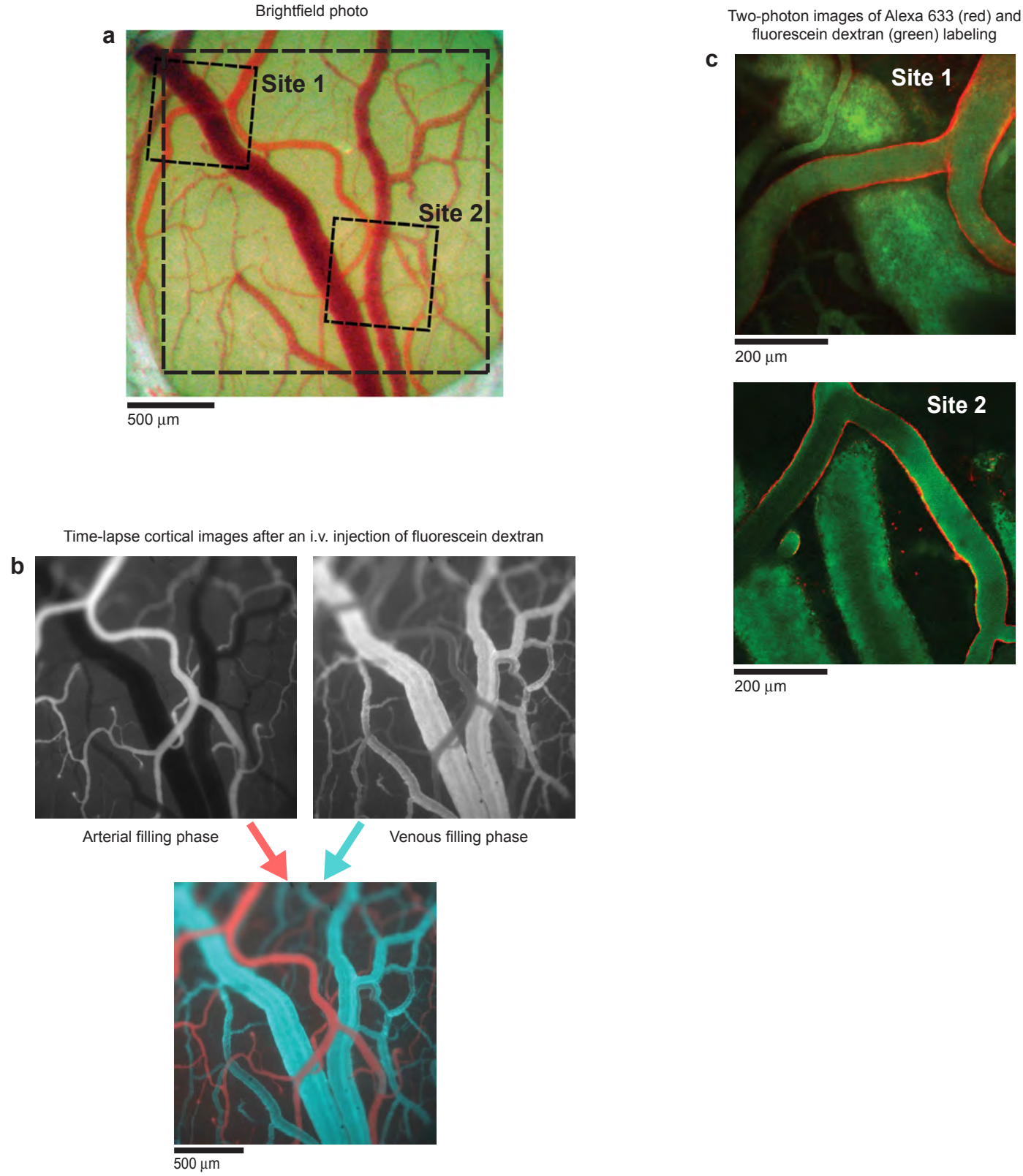

Supplementary Figure 1
Delay between the filling of arteries and veins after intravenous dye injection confirms artery specificity of Alexa 633 labeling *in vivo*

(**a**) Brightfield image of a craniotomy over the cat visual cortex, viewed through a surgical dissecting microscope. No dyes were present in the circulation at this phase of the experiment. Arteries and veins were classified based on small difference in hue—arteries orange and veins purple. These differences can be enhanced by using the 'Auto Levels' function in Adobe Photoshop, as done in panel **a** of this figure and the brightfield images shown in Supplementary Figs. 2–3. Large dashed square indicates the region imaged in **b** with a monochrome CCD camera and the two smaller square boxes (sites 1 and 2) are sub-regions corresponding to two-photon images shown in **c**.

(**b**) Time-lapse epifluorescence imaging of cortical vessels immediately after fluorescein dextran was injected intravenously in the femoral vein. The upper panels display two still images from Supplementary Video 1. The left panel was captured shortly after the dye reached the cortex when only the arteries were labeled—because the dye must pass from the femoral vein (in the leg) through the heart to get to the cerebral cortex, the arteries must label first. The right panel, captured 7 seconds later—when the dye was predominantly in the veins. Because it takes a few circulatory cycles for the dye to become equally distributed in the blood plasma, the arteries darken as the dye moves into the veins. The bottom panel is an RGB image created by overlaying the top two panels. The pixel intensity values from the arterial phase (left panel) are displayed in the red channel and those from the venous phase (right panel) in the green and blue channels—hence the cyan shading for veins.

(**c**) Two-photon images corresponding to the sites identified in **a**, after intravenous injection of Alexa 633 and fluorescein dextran. The subset of vessel walls labeled with Alexa 633 (red) correlate precisely with the classification of arteries by the two independent methods shown in **a** and **b**. The two-photon image from site 1 is an average intensity 100-µm-*z*-projection through the cortex while the two-photon image from site 2 is a single imaging plane on the cortical surface.

Hue differences between arteries and veins (as shown in panel **a**) were consistently observed across all three species examined: cat—Supplementary Fig. 1, rat—Supplementary Figs. 2-3, and mouse (data not shown).

Supplementary Figure 2
Vessel classification using brightfield vs. two-photon fluorescein dextran + Alexa 633 *in vivo*

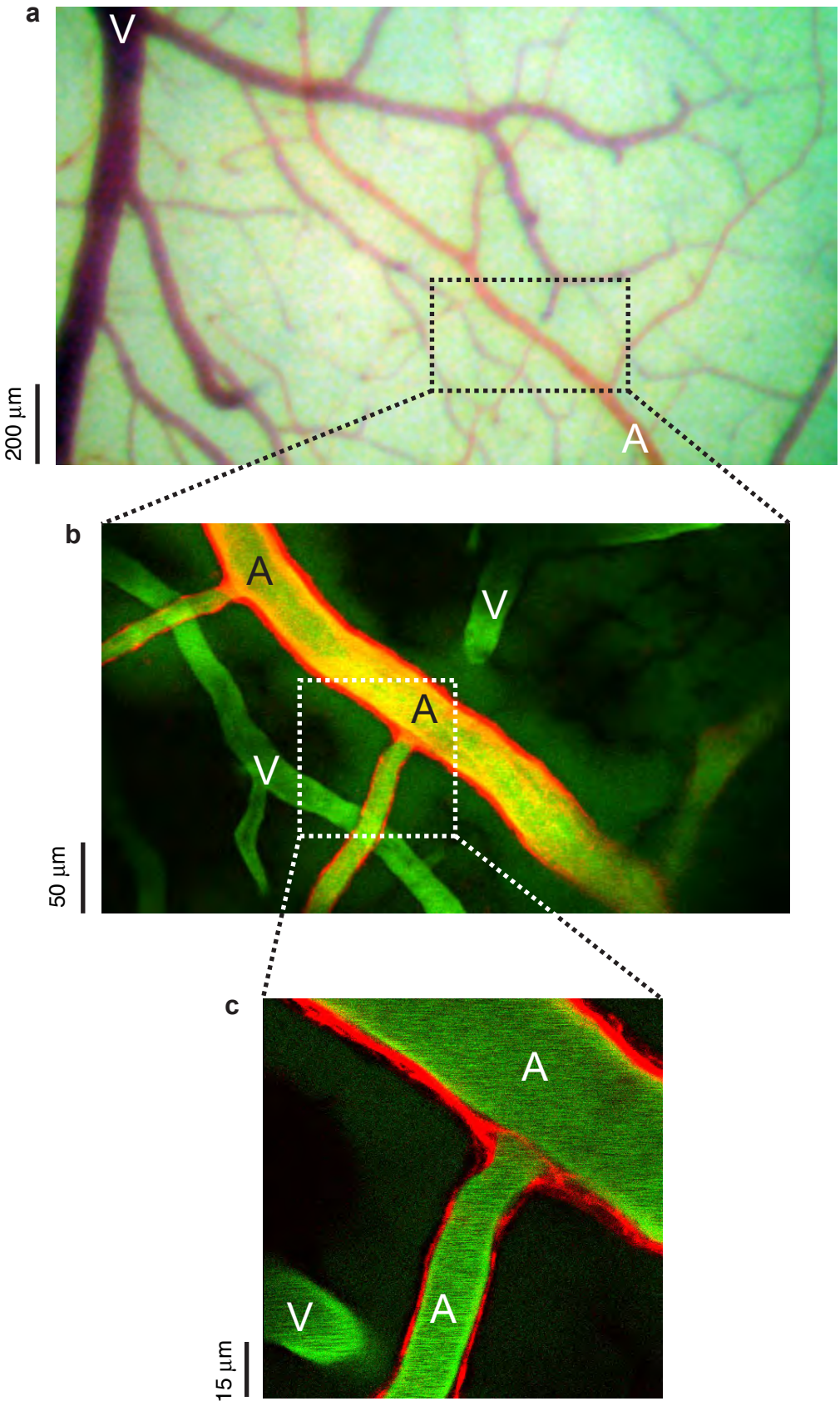

Supplementary Figure 2
Vessel classification using brightfield vs. two-photon fluorescein dextran + Alexa 633 *in vivo*

(**a**) Brightfield image of a craniotomy over rat visual cortex, equivalent to the approach described for cat visual cortex in Supplementary Fig. 1. Orange arteries (A) and purple veins (V) are readily discernable.

(**b**) Two-photon image of a sub-region shown in **a**, after intravenous injection of Alexa 633 and fluorescein dextran. Image is a 46 μm maximum intensity *z* projection and shows an arteriole (A) and daughter branches labeled with Alexa 633. A venule (V) running in parallel to the larger arteriole is not labeled by Alexa 633.

(**c**) Higher zoom two-photon image corresponding to a sub-region shown in **b**. The image is from a single imaging plane corresponding to the *z* stack shown in Supplementary Video 2. The arteriole branches are well labeled with Alexa 633 while the nearby venule is unlabeled.

Supplementary Figure 3
Vessel classification using brightfield vs. two-photon green tomato lectin + Alexa 633 *in vivo*

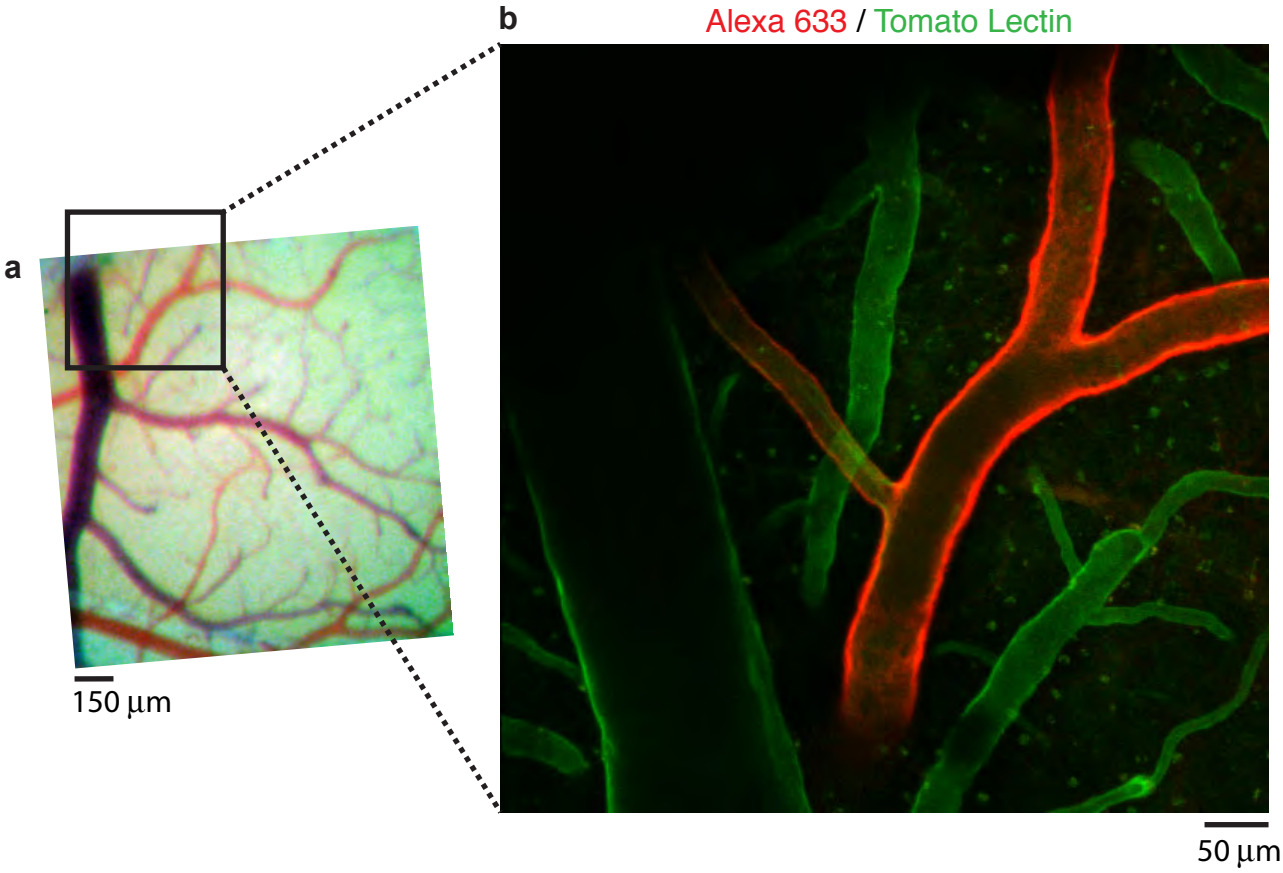

Supplementary Figure 3
Vessel classification using brightfield vs. two-photon green tomato lectin + Alexa 633 *in vivo*

(**a**) Brightfield image of a craniotomy over rat visual cortex, equivalent to the approach described in Supplementary Figs. 1–2. Orange arteries and purple veins are readily discernable.

(**b**) Two-photon image of a sub-region shown in **a**, after intravenous injection of Alexa 633 and green tomato lectin. Endothelial cells in all vessels were labeled with green tomato lectin but only arteriole branches were labeled by the Alexa 633 injection. Image is an average intensity 64-µm-*z*-projection.

Supplementary Figure 4
Persistent *in vivo* Alexa 633 labeling > 24 hours post-injection

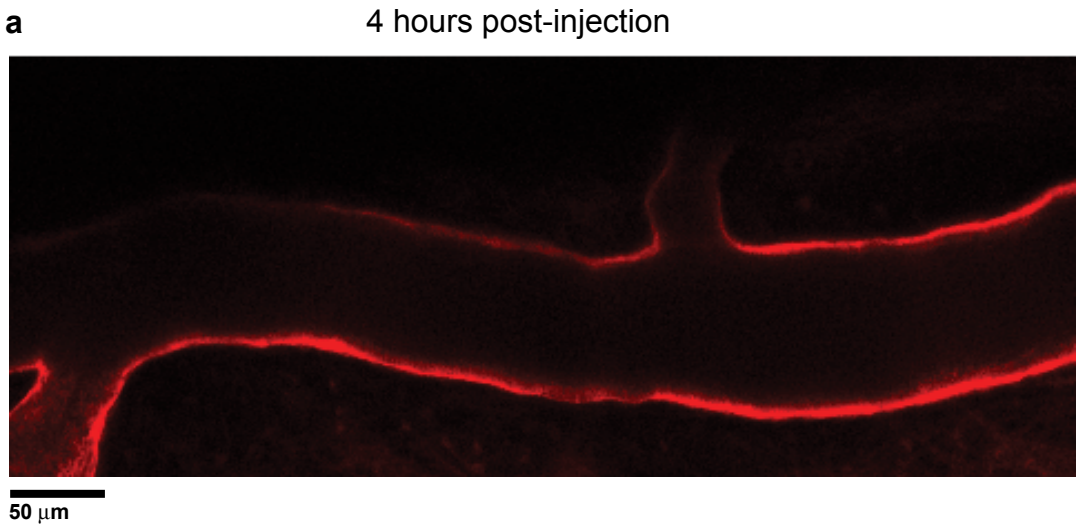

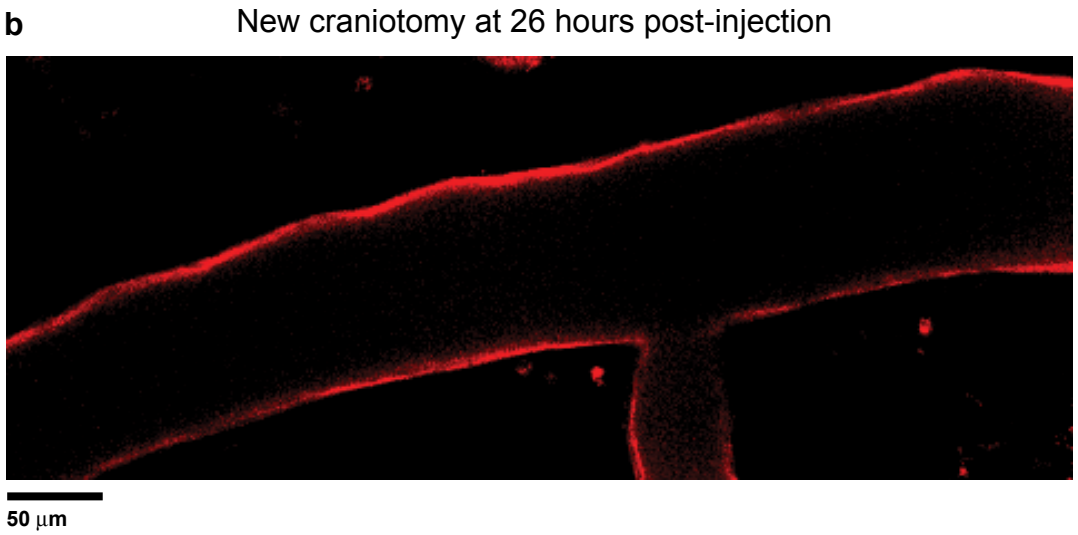

Supplementary Figure 4
Persistent *in vivo* Alexa 633 labeling > 24 hours post-injection

(**a**) Two-photon image from the cat visual cortex obtained four hours after intravenous injection of Alexa 633 is an average intensity 20-µm-*z*-projection and shows a cortical artery brightly labeled with Alexa 633.

(**b**) Another two-photon image (average intensity 10-µm-*z*-projection) showing a different cortical artery in the same cat as shown in **a**. In a given craniotomy, tissue growth over the cortex (especially in cats) reduces overall imaging quality over long time periods (24 h). Therefore to ensure that we only measured the loss in Alexa 633 wall labeling, we opened a new craniotomy 26 h after the injection and imaged a new artery. The vessel was still brightly labeled.

Images shown in **a** and **b** were obtained with the identical laser power and PMT value.

Supplementary Figure 5
Surface and penetrating arterioles ≥ 15 μm in diameter are labeled *in vivo* by Alexa 633 while veins, venules, and microvessels are not

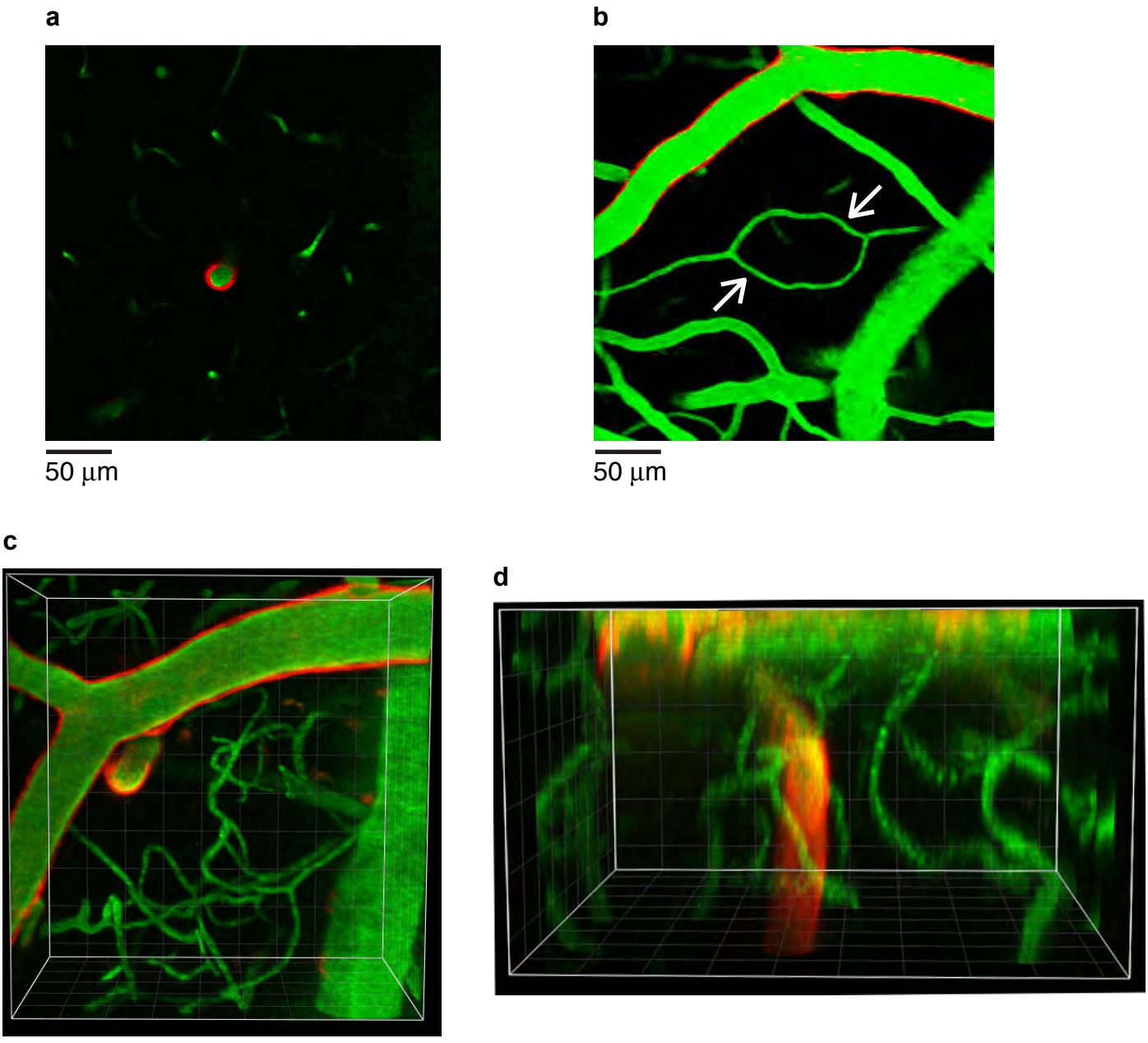

Supplementary Figure 5
Surface and penetrating arterioles ≥ 15 µm in diameter are labeled *in vivo* by Alexa 633 while veins, venules, and microvessels are not

(**a**) Single *z* plane two-photon image from mouse visual cortex, 78 µm below the pial surface. The entire vasculature is visible (green) after an intravenous injection of fluorescein dextran. The wall of a penetrating arteriole is clearly labeled with Alexa 633 (red) while surrounding micro-vessels are not.

(**b**) A surface two-photon image of a large arteriole labeled with Alexa 633. Surrounding venules and micro-vessels are not labeled by Alexa 633. Note the hexagonal microvessel loop (white arrows), as described by Blinder and colleagues (*Proc. Natl. Acad. Sci. USA* 2010). The image is a maximum intensity 15-µm-*z*-projection, from the same craniotomy used to obtain the image shown in **a**.

(**c**) Dorsal view perspective of a 3D volume rendering of the nearly identical region shown in **a**, but with a higher 2× optical zoom. The surface and penetrating arterioles are labeled by Alexa 633 while the vein on the right edge and microvessels are not.

(**d**) Left side view perspective of the same 3D volume shown in **c.** The penetrating arteriole is labeled throughout the imaged depth.

In the current example, Alexa 633 labeling was obtained by local micropipette injection (cf. intravenous injection in experiments shown in Supplementary Figs. 1–4).

x-*y*-*z* volume dimensions in **c**–**d**: 220 × 234 × 123 µm. A 360° rendering of the volume is shown in Supplementary Video 3.

Supplementary Figure 6
The smallest surface arteriole branches (≤ 10 μm diameter) are not labeled by Alexa 633 *in vivo*

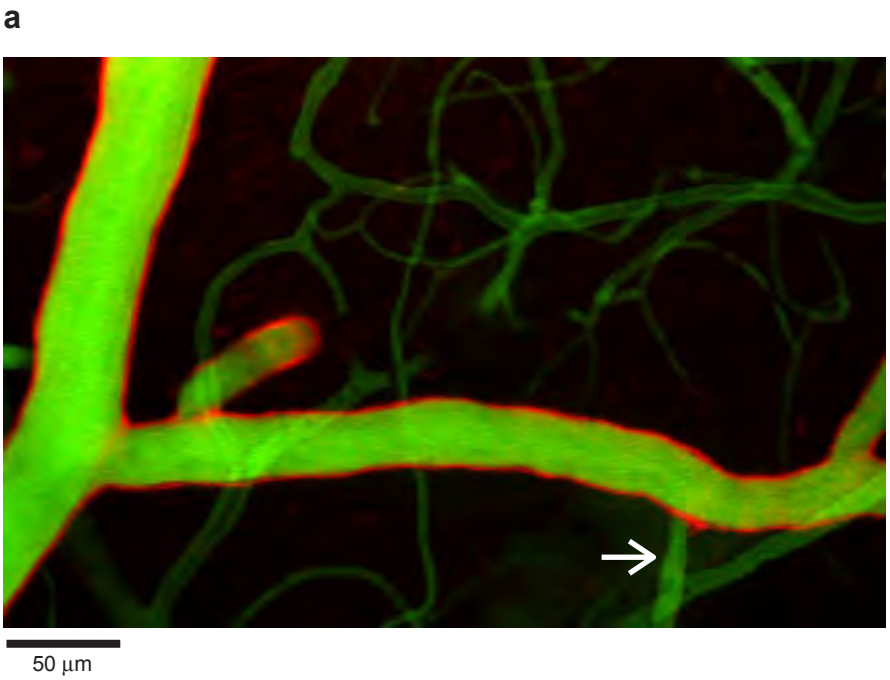

Supplementary Figure 6
The smallest surface arteriole branches (≤ 10 µm diameter) are not labeled by Alexa 633 *in vivo*

(**a**) Average intensity 66-µm-*z*-projection two-photon image from mouse visual cortex. The entire vasculature is visible (green) after an intravenous injection of fluorescein dextran. The smallest surface arteriole branch ≈ 10 µm diameter (white arrow) is unlabeled by local micropipette injection of Alexa 633.

(**b**) Average intensity 12-µm-*z*-projection two-photon image from rat visual cortex. After intravenous injection of Alexa 633, the ≈ 25-µm-diameter arteriole was labeled. But the smaller ≈ 7-µm-diameter offshoot was not labeled by Alexa 633 (white arrow). Alexa 633 labeling ends abruptly at the vessel branch point (red arrow). The vasculature lumen is visible (green) via an intravenous injection of fluorescein dextran.

Supplementary Figure 7
A deep penetrating arteriole labeled by Alexa 633 *in vivo*

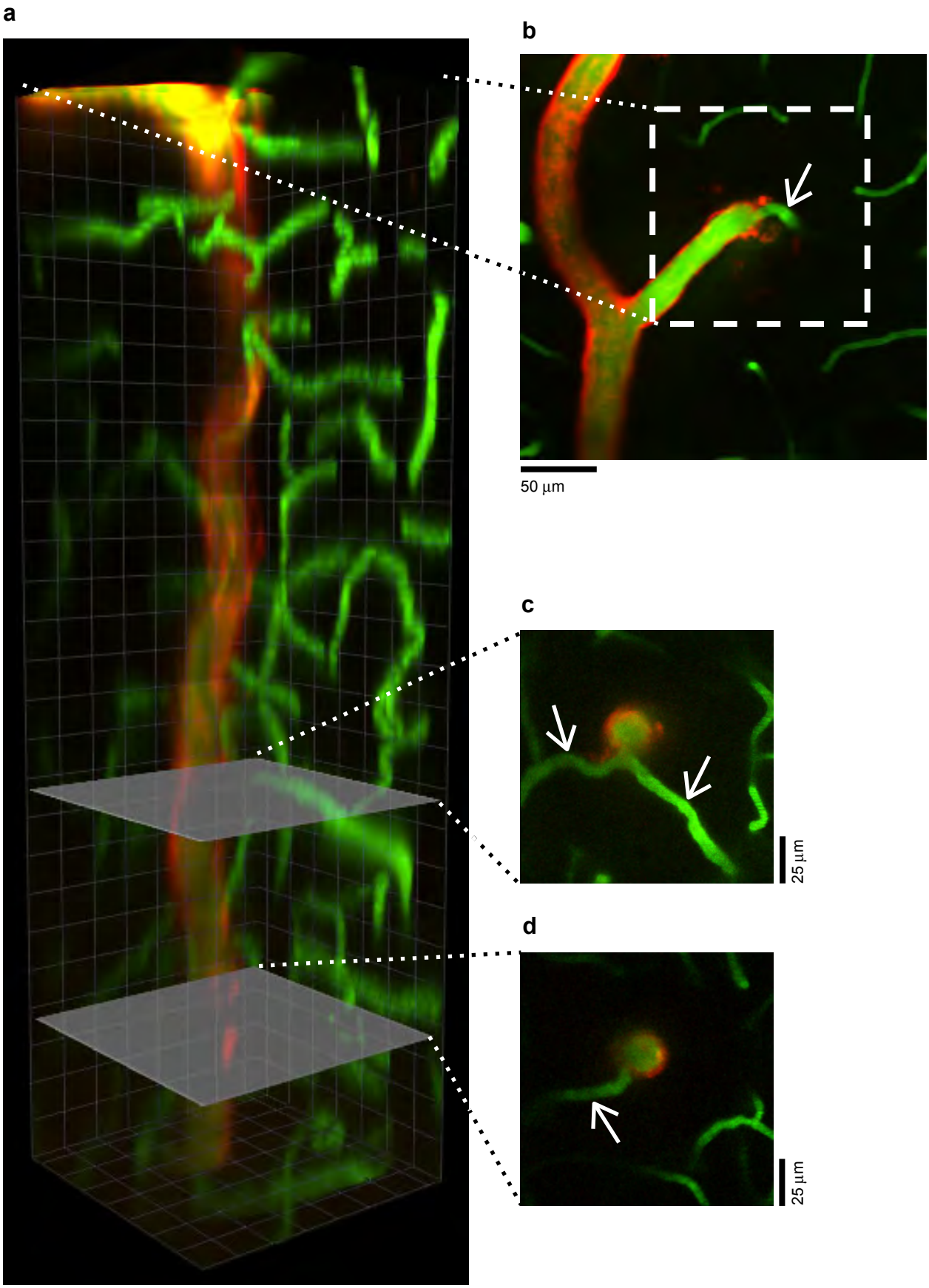

Supplementary Figure 7
A deep penetrating arteriole labeled by Alexa 633 *in vivo*

(**a**) Side view perspective of a 3D volume rendering of a two-photon imaged site in rat visual cortex—from the pial surface to a depth of 550 µm. The lumen of all vessels is labeled with fluorescein dextran (green). After intravenous injection of Alexa 633, a penetrating arteriole ≈ 17-µm-diameter is labeled with Alexa 633 (red) while the surrounding micro-vessels are not. *x*-*y*-*z* volume dimensions: 135 × 135 × 550 µm. Gray slices correspond to *z* cross-sections shown in **c** and **d**.

(**b**) Dorsal view of the same cortical region shown in **a**. The dashed white square indicates the sub-region used to render the 3D volume shown in **a**. The white arrow shows a small branch coming off the larger ≈ 17-µm-diameter penetrating arteriole. This small branch (≤ 10 µm diameter) is not labeled by the intravenous injection of Alexa 633.

(**c**) Image of a maximum intensity 30-µm-*z*-projection centered 355 µm below the cortical surface. The penetrating arteriole is labeled by Alexa 633 while two small < 10-µm-diameter branches (white arrows) and surrounding micro-vessels are not.

(**d**) Image of a maximum intensity 20-µm-*z*-projection centered 480 µm below the cortical surface. The penetrating arteriole is still labeled by Alexa 633 while the small < 10-µm-diameter branchlet (arrowed) and surrounding vessels are not.

Supplementary Figure 8
Small (< 10 µm diameter) branchlets off penetrating arterioles are not labeled by Alexa 633 *in vivo*

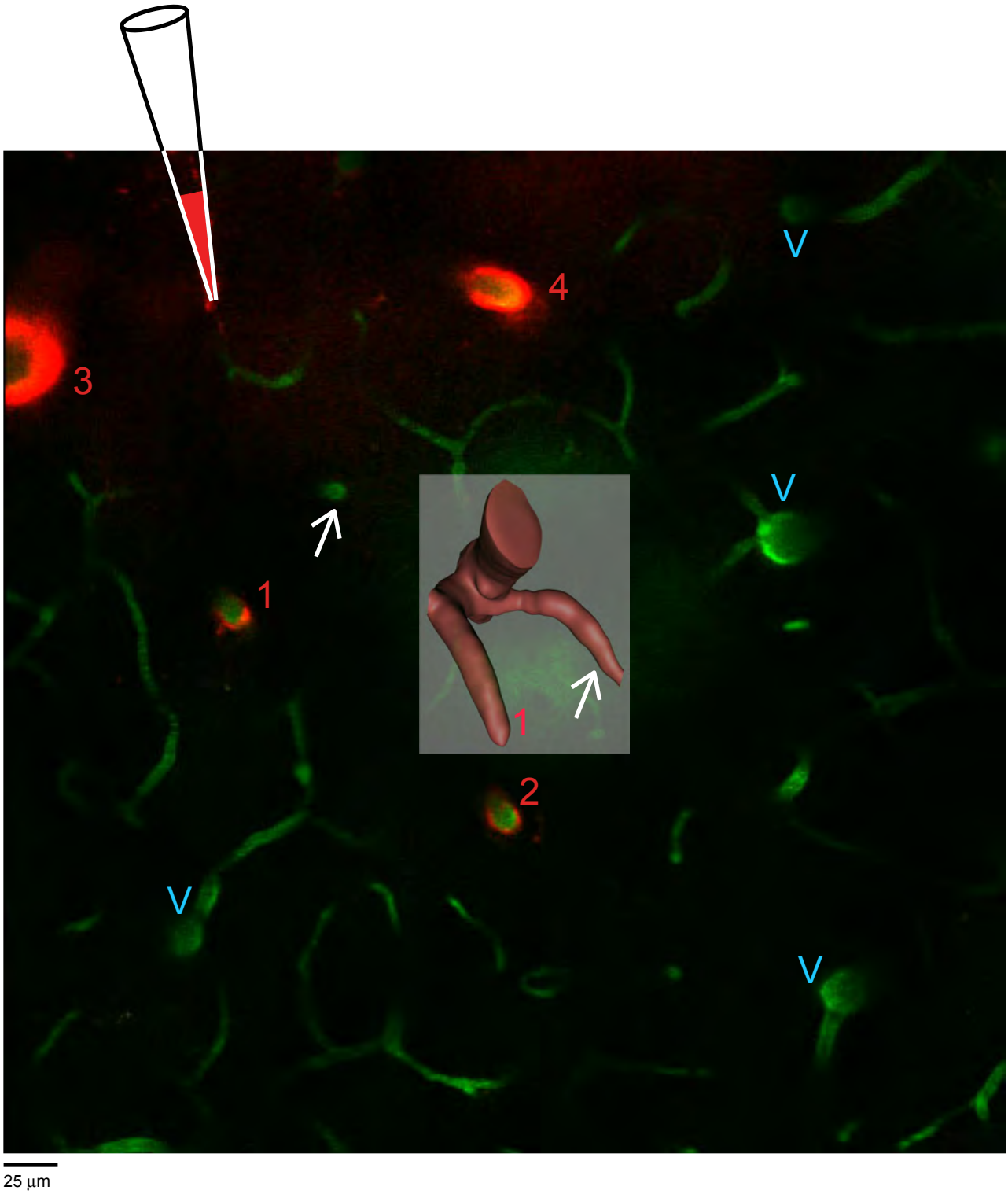

Supplementary Figure 8
Small (< 10-µm-diameter) branchlets off penetrating arterioles are not labeled by Alexa 633 *in vivo*

Two-photon image of an average intensity 16-µm-*z*-projection centered 105 µm below the pial surface. The lumen of all vessels is labeled with fluorescein dextran (green). The schematic of a micropipette indicates the tip location where Alexa 633 was ejected. Penetrating arterioles with branchlets (# 1–4) are labeled with Alexa 633 but diving venules (V) and microvessels are not. The white arrow indicates an unlabeled ≈ 8-µm-diameter branchlet from the same artery as # 1 (≈ 12 µm diameter and labeled by Alexa 633).

Inset overlaid in the center of the two-photon image provides further details where Alexa 633 labeling ends on arterioles by showing a mask rendering of the penetrating arteriole that gives rise to the two branchlets: # 1 and the other indicated by the white arrow. The mask was created using the automatic masking function in Imaris software. The best visualization of the mask of the two-branchlets with their parent arteriole was via a ventral projection (as shown).

Note that the lack of label in the ≈ 8-µm-diameter branchlet could not be due to diffusion distance from the injection site since artery # 2 is much further away from the pipette tip and is clearly labeled.

Supplementary Figure 9
PDGFR-β immunohistochemistry suggests that pericytes are not labeled by Alexa 633

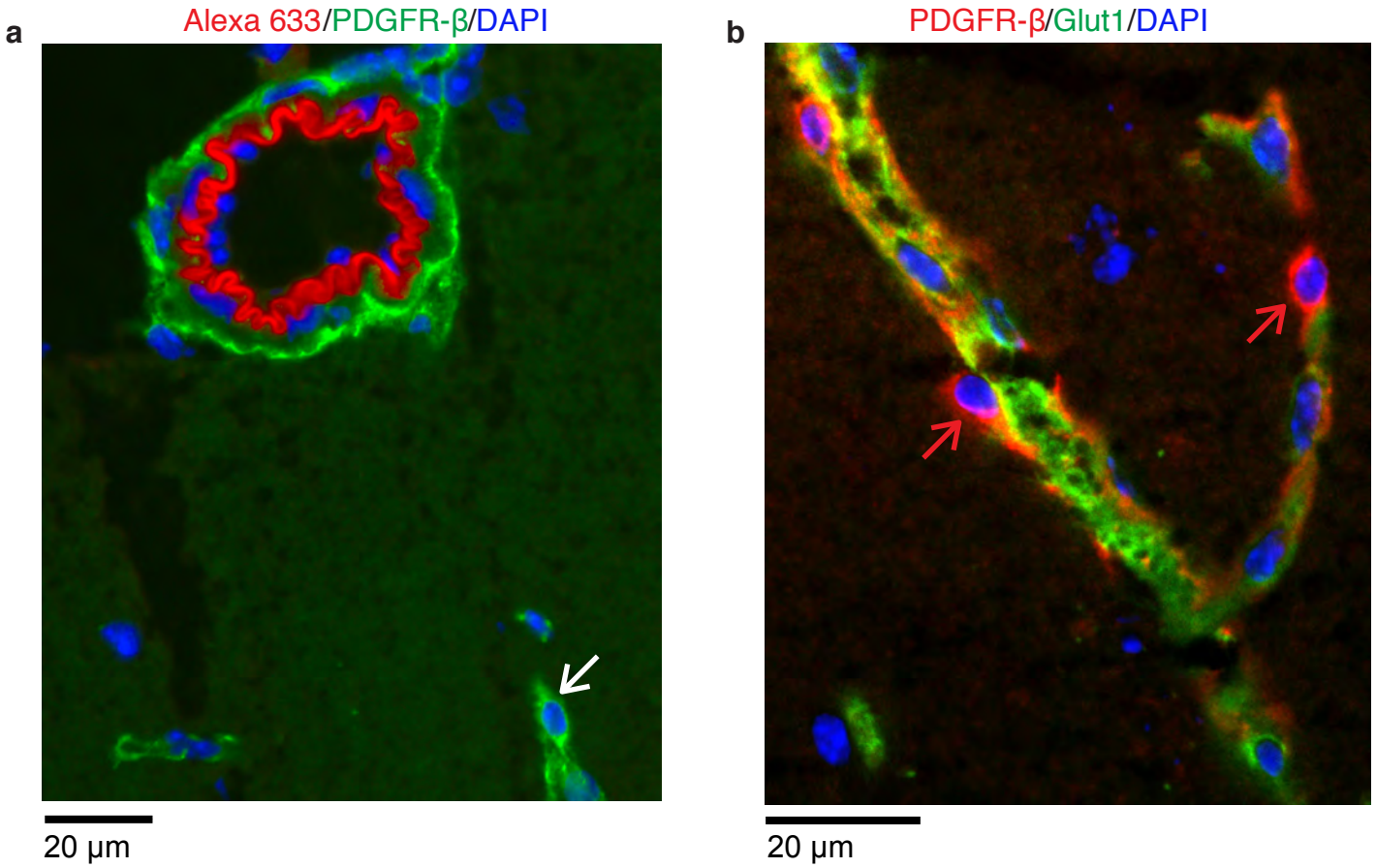

Supplementary Figure 9
PDGFR-β immunohistochemistry suggests that pericytes are not labeled by Alexa 633

(**a**) Triple labeling of Alexa 633/PDGFR-β/DAPI in mouse visual cortex shows no overlap of labeling between Alexa 633 (red) and PDGFR-β (green). Furthermore, pericytes on microvessels, e.g., white arrow, show no labeling by Alexa 633.

(**b**) Triple labeling of PDGFR-β/Glut1/DAPI in mouse visual cortex shows pericytes labeled (red) along microvessels visualized with Glut1 (green).

We present numerous lines of *in vivo* and other histological data to show that there is no labeling of Alexa 633 on microvessels < 10 μm in diameter (also see Supplementary Figs. 5–8, 10). Furthermore, there are no pericytes in the aorta (Wagenseil and Mecham, *Physiol. Rev.* 2009), yet Alexa 633 labels distinct elastin bands in the aorta (Supplementary Fig. 15). The labeling of Alexa 633 is inconsistent with pericytes as a target.

Supplementary Figure 10
Alexa 633 does not label the small microvessels in histological sections of the cerebral cortex

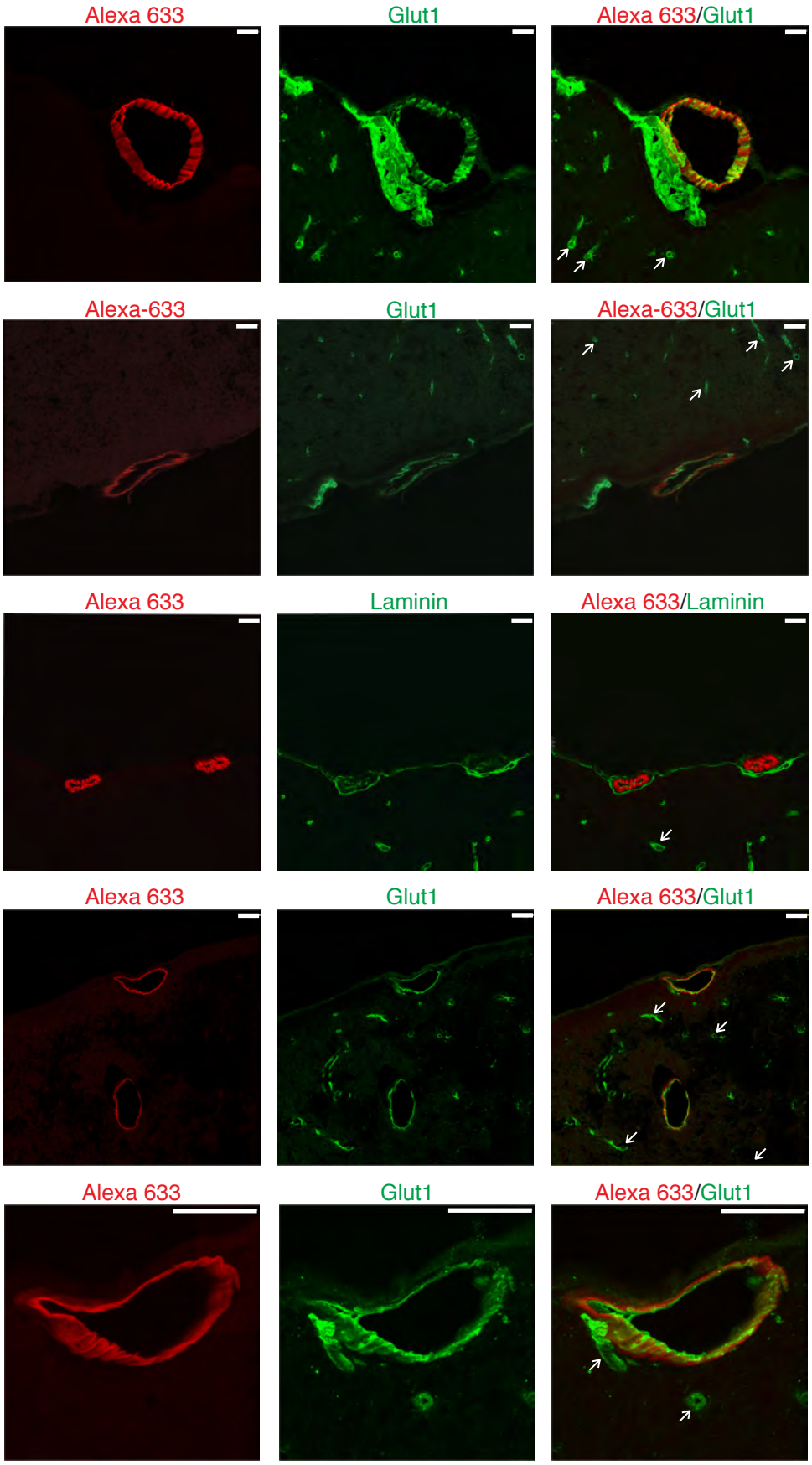

Supplementary Figure 10
Alexa 633 does not label the small microvessels in histological sections of the cerebral cortex

Glut-1 or Laminin were used as a green counterstain for microvessels (white arrows) in individual tissue sections. Not a single microvessel was co-labeled by Alexa 633 (red). All data shown are from mouse visual cortex. Scale bars = 20 μm.

Supplementary Figure 11
Arterioles but not venules in the visual cortex respond to drifting grating visual stimuli

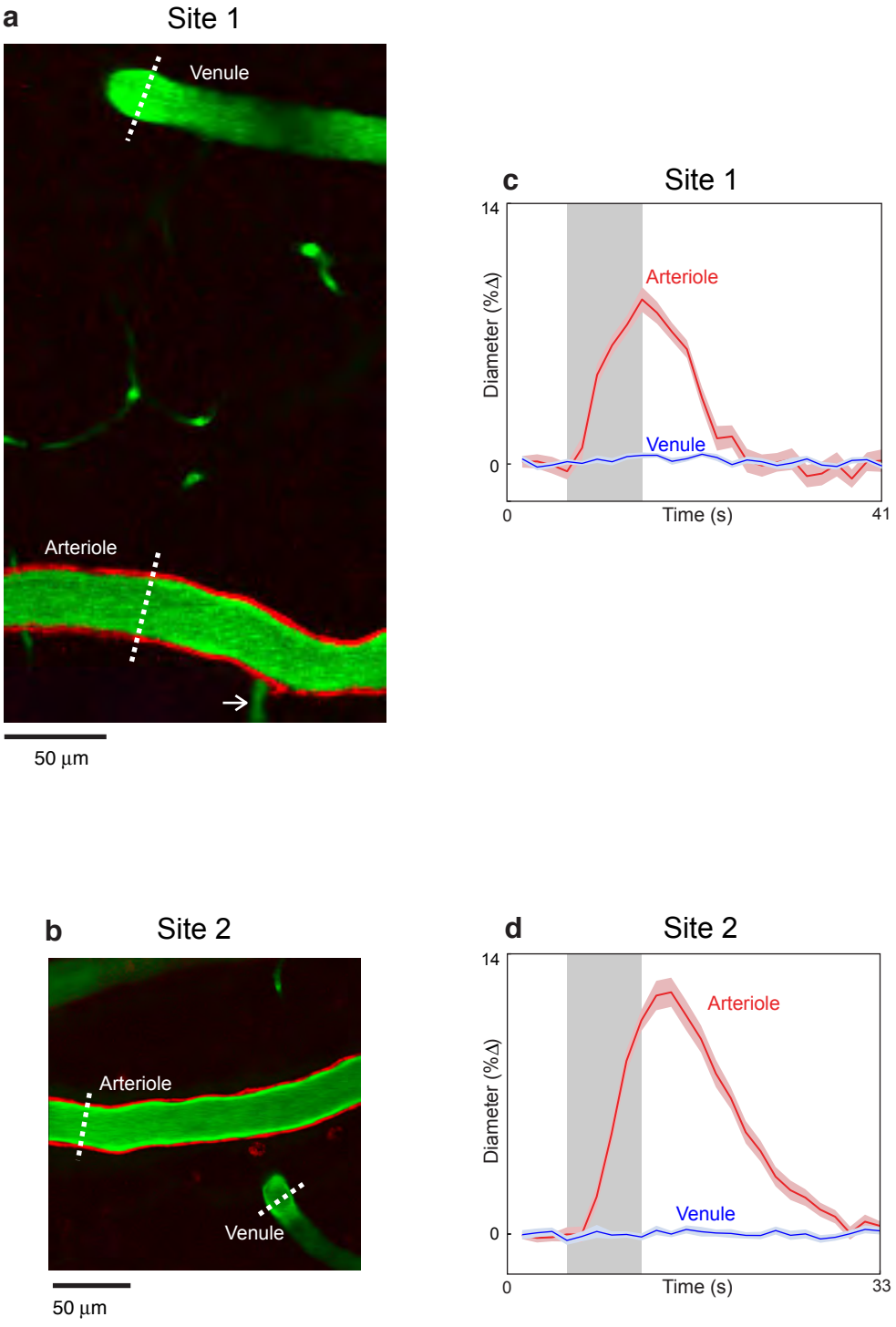

Supplementary Figure 11
Arterioles but not venules in the visual cortex respond to drifting grating visual stimuli

(**a**–**b**) Two-photon images collected from two adjacent cortical sites in the same mouse. The vascular lumen (green) was labeled by intravenous injection of fluorescein dextran. A single micropipette injection of Alexa 633 (red) selectively labeled arterioles in both sites. White hatched lines correspond to the cross-sections used to analyze the time course of change in vessel diameter with sensory stimulation (**c**–**d**). White arrow in **a** denotes the ≤ 10-μm-diameter arteriole branchlet that was not labeled by Alexa 633.

(**c**–**d**) Time courses of percent change in the vessel diameter to visual stimulation for arterioles (red traces) and venules (blue traces) recorded simultaneously in each of the two sites using two-photon microscopy. The grey shaded rectangle denotes the period of visual stimulation. Each time course is shown as an average of twenty-four trials to a drifting grating visual stimulus. Error bands represent s.e.m. At both imaged sites, arterioles showed large sensory stimulus evoked responses. Venules were unresponsive to visual stimulation—they never showed visually-evoked responses: ANOVA test was always $P > 0.05$ across blank and n test visual stimuli, the percentage change of visually-evoked dilation was always < 1%, and visually-evoked dilations never exceeded three standard deviations above the mean pre-stimulation baseline.

Supplementary Figure 12
Neuronal responses are unaffected by local micropipette application of Alexa 633 in the visual cortex

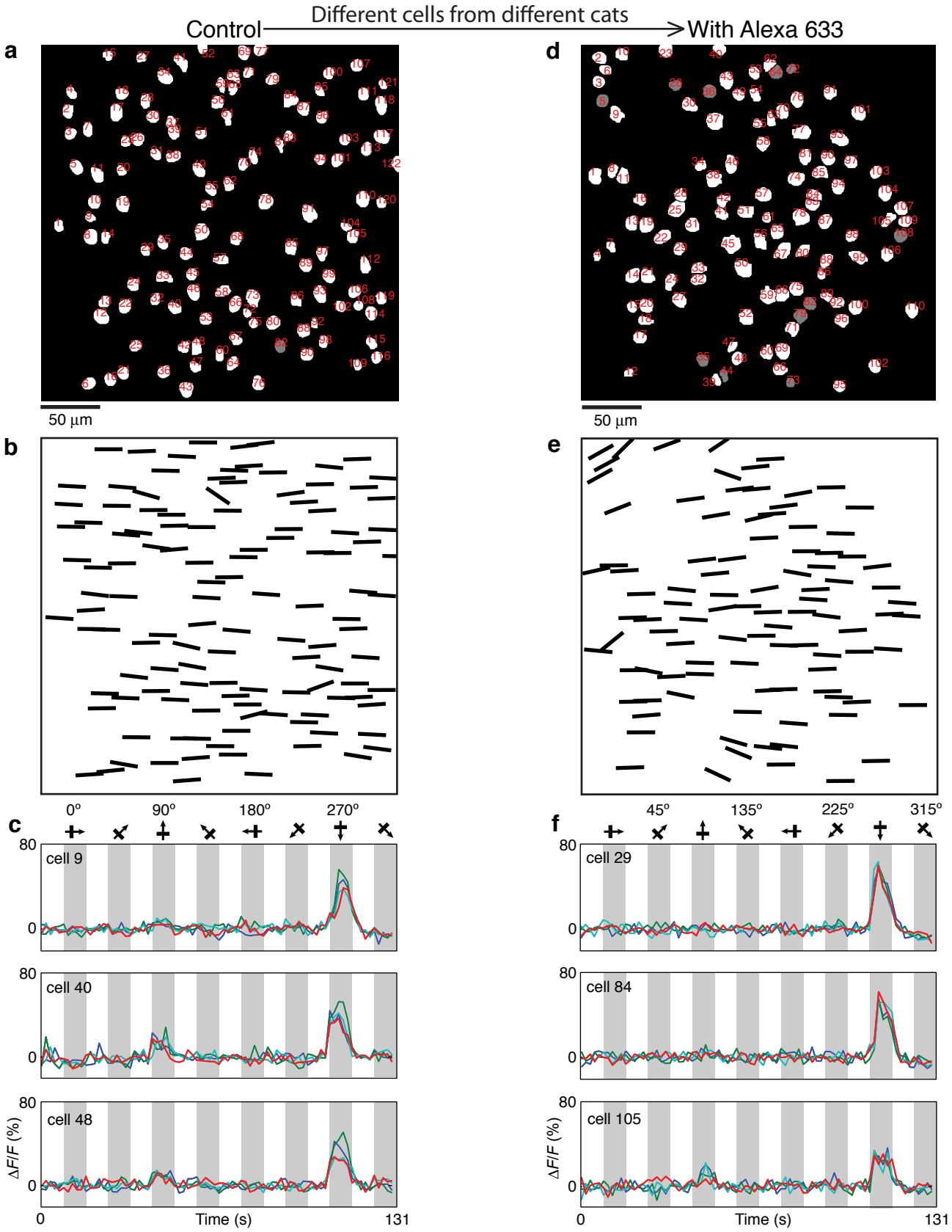

Supplementary Figure 12
Neuronal responses are unaffected by local micropipette application of Alexa 633 in the visual cortex

(**a–c**) Masks of identified somata, local orientation map, and time course of calcium transients from a control cat (no Alexa 633 applied). Calcium transients were measured after bulk loading Oregon Green 488 Bapta-1 AM (OGB 1-AM).

(**d**–**f**) Data from another cat, but here Alexa 633 was co-injected with OGB 1-AM. Cell numbers listed in time courses (**c**,**f**) match corresponding numbers shown for somata masks (**a**,**d**). For the cell masks shown in **a** and **d**, cells painted in white were significantly tuned for orientation and cells painted in gray were untuned. Each time course in **c** and **f** show individual cell responses—four trials superimposed.

Greater than 90% of neurons in cat visual cortex were visually responsive both in 'control' (where no Alexa 633 was co-injected with the calcium indicator) and Alexa 633 injected animals. The orientation selectivity index (OSI) of neurons was indistinguishable between control and Alexa 633 animals (control OSI = 0.736 ± 0.014 vs. Alexa 633 OSI = 0.737 ± 0.019, mean ± s.e.m; control n = 120 cells, Alexa 633 n = 110 cells; P = 0.46 Mann-Whitney). Cats have distinct iso-orientation domains and thus OGB 1-AM can be injected into specific orientation domains guided by intrinsic signal optical imaging. We deliberately chose cortical locations in control and Alexa 633 treated sites in cat visual cortex that had the same overall orientation and direction preference—to avoid domain-based differences (cardinal stimulus orientations over-represented in visual cortex).

Supplementary Figure 13
Neuronal responses are unaffected before and after intravenous application of Alexa 633 in the same animal

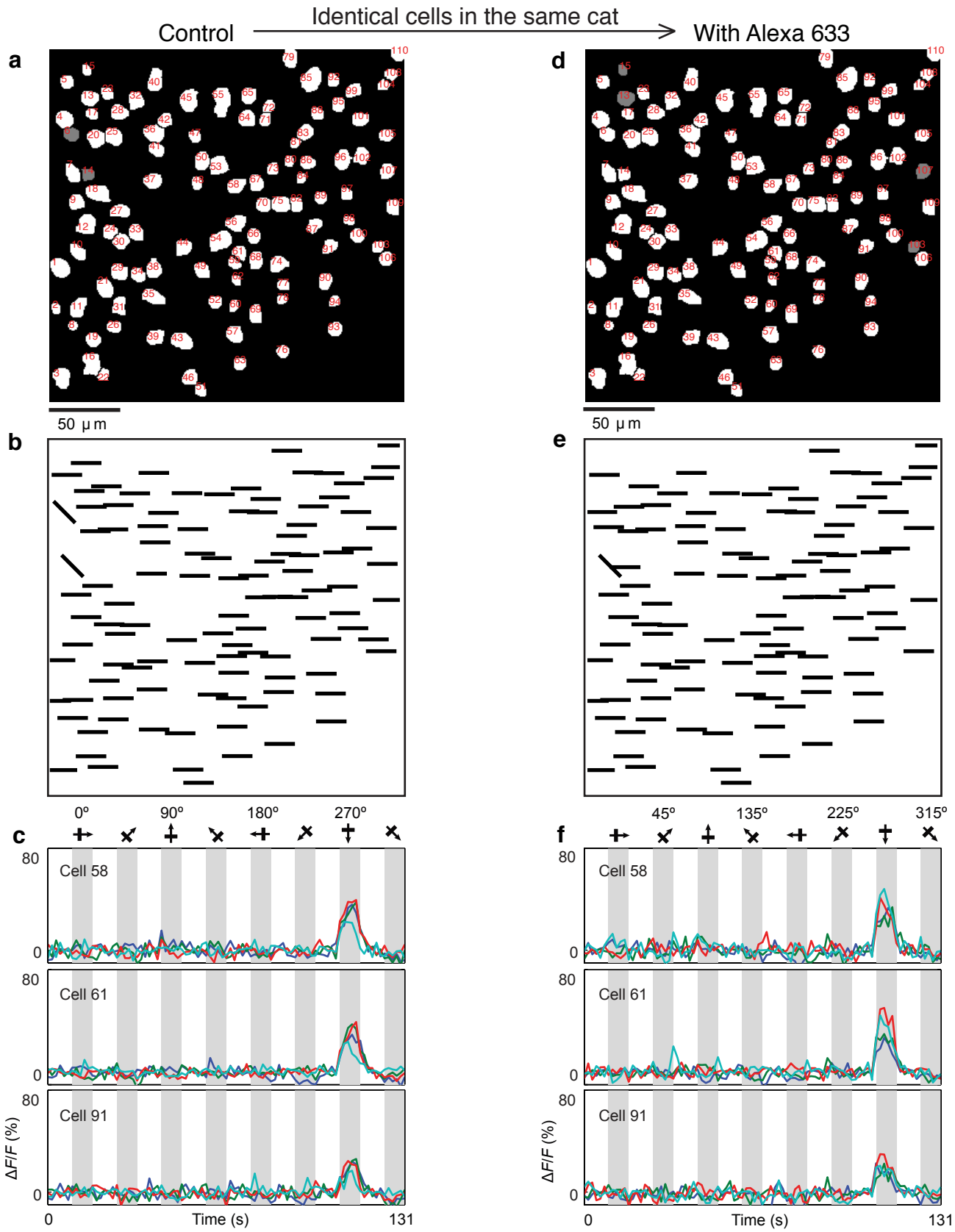

Supplementary Figure 13
Neuronal responses are unaffected before and after intravenous application of Alexa 633 in the same animal

(**a**–**c**) Masks of identified somata, local orientation map, and time course of calcium transients before Alexa 633 was applied. Calcium transients were measured after bulk loading Oregon Green 488 Bapta-1 AM (OGB 1-AM).

(**d**–**f**) Data from same cat—exactly the same cells as shown in **a**–**c**, but after Alexa 633 was applied intravenously (femoral vein). Cell numbers listed in time courses (**c**,**f**) match corresponding numbers shown for somata masks (**a**,**d**). For the cell masks shown in **a** and **d**, cells painted in white were significantly tuned for orientation and cells painted in gray were untuned. Each time course in **c** and **f** show individual cell responses—four trials superimposed. For the identical neurons, before and after Alexa 633 application injected showed no difference in the amplitude of visually evoked responses (control amplitude $\Delta F/F = 16.52 \pm 0.69$ % vs. Alexa 633 amplitude $\Delta F/F = 15.93 \pm 0.71$ %, mean ± s.e.m; $n = 105$ cells; $P = 0.22$ Wilcoxon signed rank test) and orientation selectivity index (control OSI = 0.880 ± 0.012 vs. Alexa 633 OSI = 0.867 ± 0.014, mean ± s.e.m; $n = 105$ cells; $P = 0.43$ Wilcoxon signed rank test).

Supplementary Figure 14
EEG and heart rate are unaffected by Alexa 633

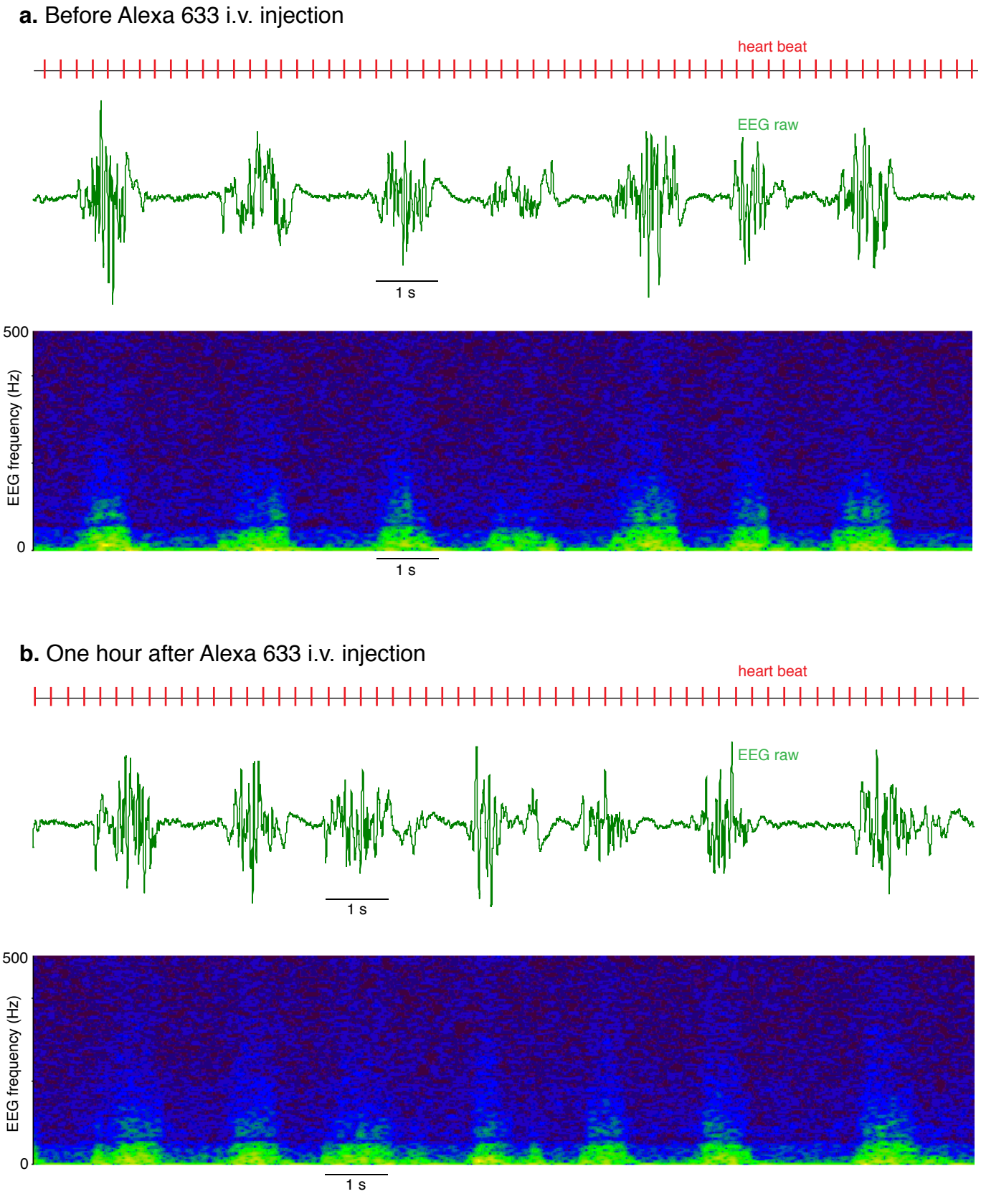

Supplementary Figure 14
EEG and heart rate are unaffected by Alexa 633

(**a**) Heart beat, raw EEG traces, and spectrogram of EEG records before intravenous injection of Alexa 633 in an anesthetized and paralyzed cat.

(**b**) Heart beat, raw EEG traces, and spectrogram of EEG records after intravenous injection of Alexa 633 (1 mg kg^{-1}) in the same anesthetized and paralyzed cat used to collect the data shown in **a**.

No difference in heart rate and EEG activity was observed before and after Alexa 633 injection. Alexa 633 labeling of arterioles was visible when data shown in **b** were collected.

Supplementary Figure 15
Binding site of Alexa 633 on artery/arteriole wall

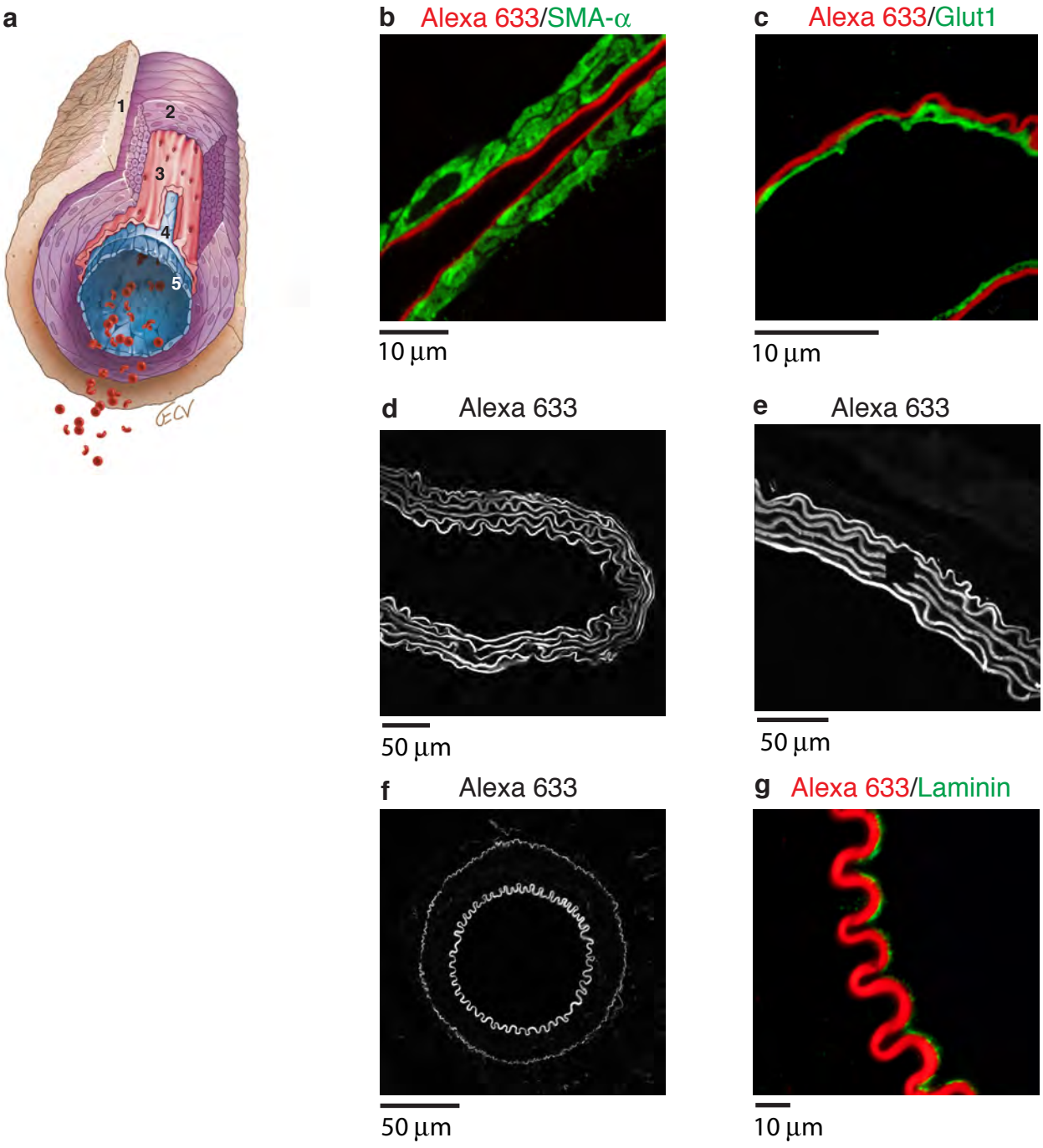

Supplementary Figure 15
Binding site of Alexa 633 on artery/arteriole wall

(**a**) Schematic of the five distinct layers in the brain arteriole wall: **1**. Outermost covering containing collagen, **2**. smooth muscle, **3**. elastin fibers, **4**. endothelial basement membrane, **5**. endothelial cells.

(**b**) Anti-SMA-α (green) was used to label smooth muscle in brain arterioles. Anti-SMA-α shows no overlap with Alexa 633 (red) labeling. Data shown are from macaque monkey but identical results were obtained in rodents.

(**c**) Anti-Glut1 (green) was used to label endothelial cells in brain arterioles—no overlap with Alexa 633 labeling. Data shown are from mouse but identical results were obtained in other species. Images shown in **b**, **c, g** were collected with sequential scanning confocal microscopy.

(**d**) Alexa 633 labeled six characteristic elastin fiber layers in mouse aorta, images collected by using low (2 mW) two-photon laser power.

(**e**) Higher zoom of mouse aorta also collected using low two-photon laser power. Black square within the center of the labeled arteriole wall is from a preceding intentional high power two-photon laser bleach of Alexa 633, to demonstrate that Alexa 633 labeling was not contaminated by autofluorescence.

(**f**) The signature pattern of thin external elastic lamina and thick internal elastic lamina of mouse femoral artery was visible with Alexa 633 staining.

(**g**) Anti-laminin (green) was used to label endothelial basement membrane in mouse femoral artery. Anti-laminin staining did not overlap with Alexa 633 labeling.

The schematic shown in panel **a** was made specifically for the current publication and is an original drawing by Emma Vought, a medical illustrator in the Department of Neurosciences at the Medical University of South Carolina. The schematic is based on drawings shown in Principles of Anatomy & Physiology (13th Edition) by Tortora & Derrickson (Wiley 2012).

Supplementary Figure 16
Alexa 633 labels elastin fibers on artery walls in brain and aorta

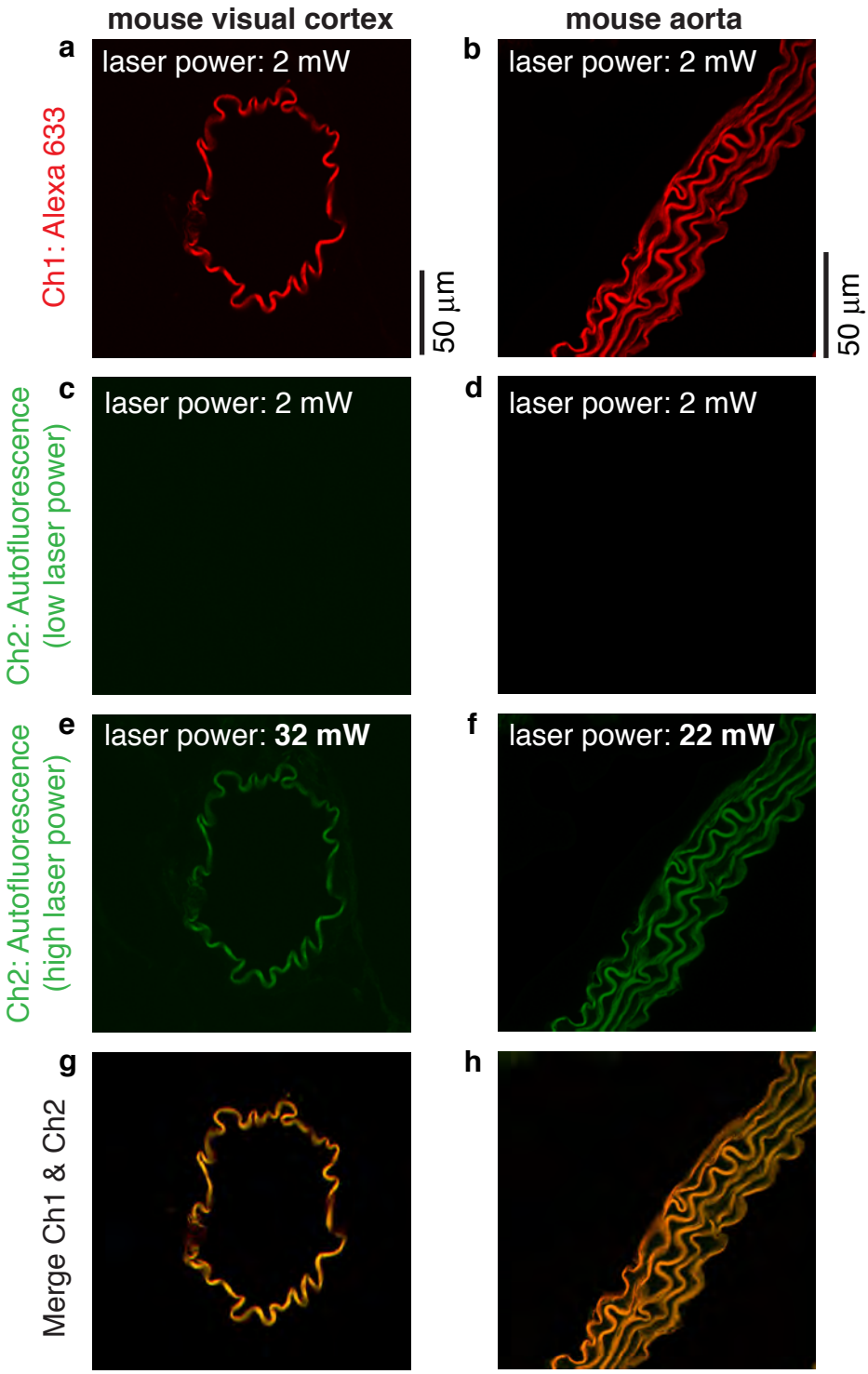

Supplementary Figure 16
Alexa 633 labels elastin fibers on artery walls in brain and aorta

(**a,b**) Two-photon images of a mouse brain arteriole and a mouse aorta labeled with Alexa 633 (laser power = 2 mW). Data collected on a red emission channel.

(**c,d**) No autofluorescence was measured from the blue-green emission channel with 2 mW laser power.

(**e,f**) Robust elastin autofluorescence was detected from the blue-green emission channel using high (22–32 mW) two-photon laser power.

(**g,h**) Alexa 633 and elastin autofluorescence on the artery wall overlapped near perfectly (Pearson's R_r = 0.84 and 0.96 in **g** and **h**, respectively).

Images shown were collected from postmortem tissue sections.

Supplementary Figure 17
Alexa 633 labeling of human aorta

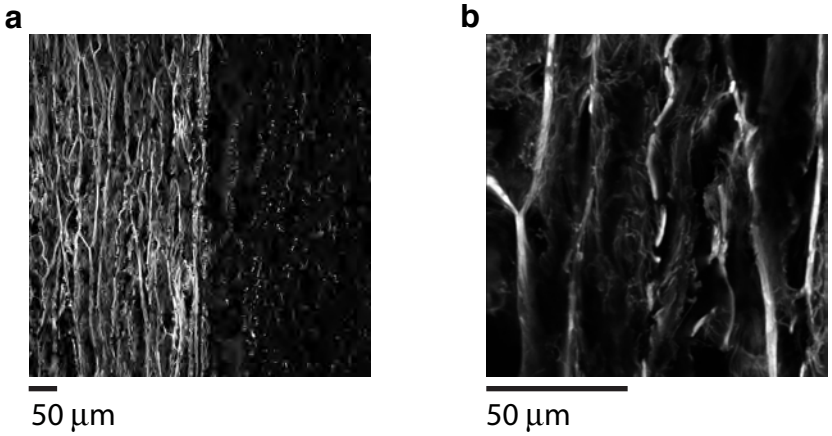

Supplementary Figure 17
Alexa 633 labeling of human aorta

(**a**) Two-photon image from a human aorta—postmortem tissue cross-section. Unlike the signature six layers of elastin fibers in mouse aorta (see Supplementary Fig. 15 d–e), the human aorta has many more tightly packed bands of elastin fibers. From left to right, the image shows Alexa 633 labeling of the tunica media of the aorta and an abrupt transition to the adventitial layer.

(**b**) Higher zoom of the tunica media shown in **a**. Individual elastin bundles of fibers were well labeled by Alexa 633. Not shown but analogous to our observations in animal tissues (see Supplementary Figs. 15–16), human tissue had no blue-green autofluorescence when using low two-photon laser power and high laser power bleached Alexa 633 labeling. Images are not background subtracted.

Supplementary Figure 18
Alexa 633 labeling of mouse kidney

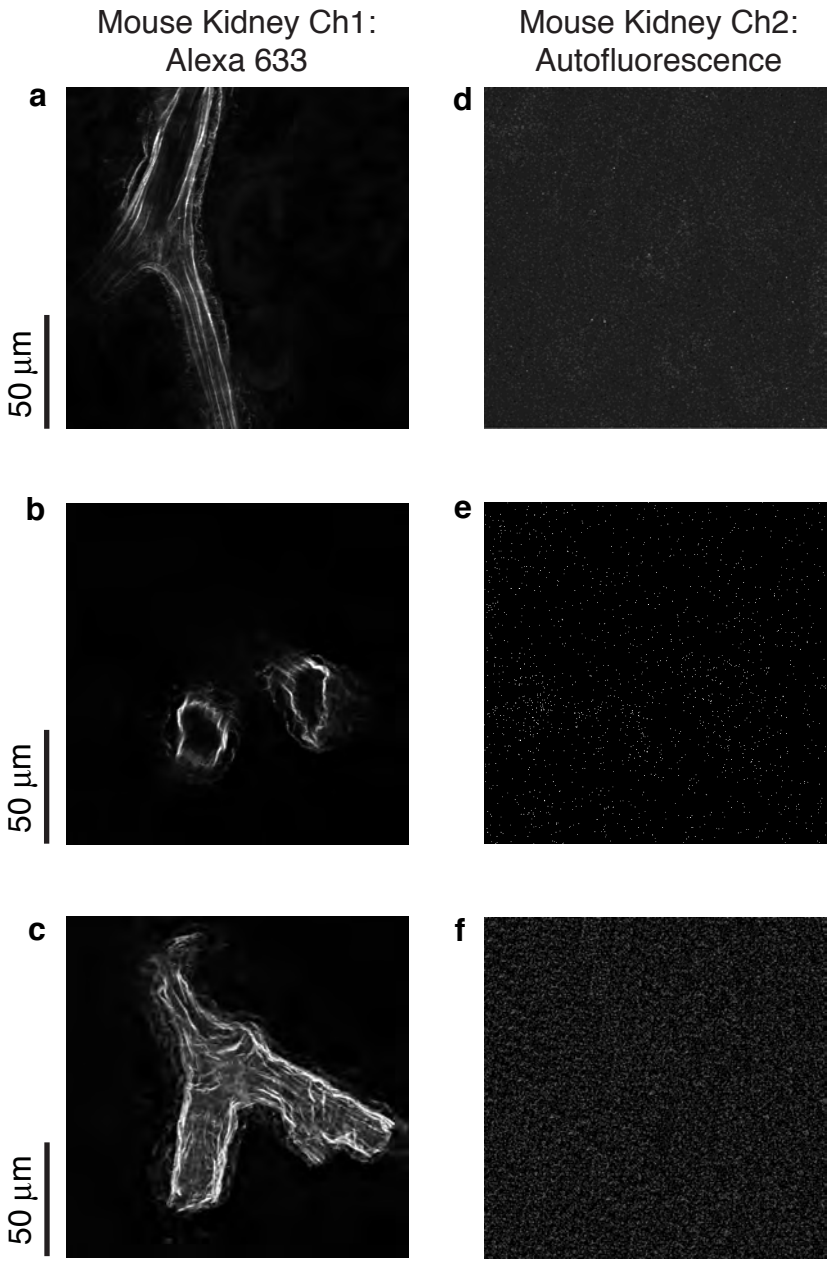

Supplementary Figure 18
Alexa 633 labeling of mouse kidney

(**a**) Two-photon image of a freshly dissected kidney (no fixative). 2 μM Alexa 633 was applied directly to the dissected kidney. An arteriole shown as a longitudinal section was brightly labeled by Alexa 633. The Alexa 633 was applied immediately after the kidney was dissected. The image was collected approximately one hour after the topical Alexa 633 application.

(**b,c**) Two-photon images from another freshly dissected kidney. But here Alexa 633 labeling was done *in vivo* by tail vein injection (1 mg kg^{-1}). An individual two-photon optical slice is shown in **b** and a maximum intensity 100-μm-*z*-projection is shown in **c**. The kidneys were removed approximately 1 hour after the tail vein injection and immediately imaged.

(**d**–**f**). No blue-green autofluorescence detected with the same laser power used to collect red channel Alexa 633 fluorescence shown in **a**–**c**. Image pairs **a**,**d**; **b**,**e**; and **c**,**f** were each collected simultaneously on two separate detector channels. Images are not background subtracted.

Supplementary Figure 19
Red blood cell velocity in cortical microvessels after intravenous injection of fluorescent dyes

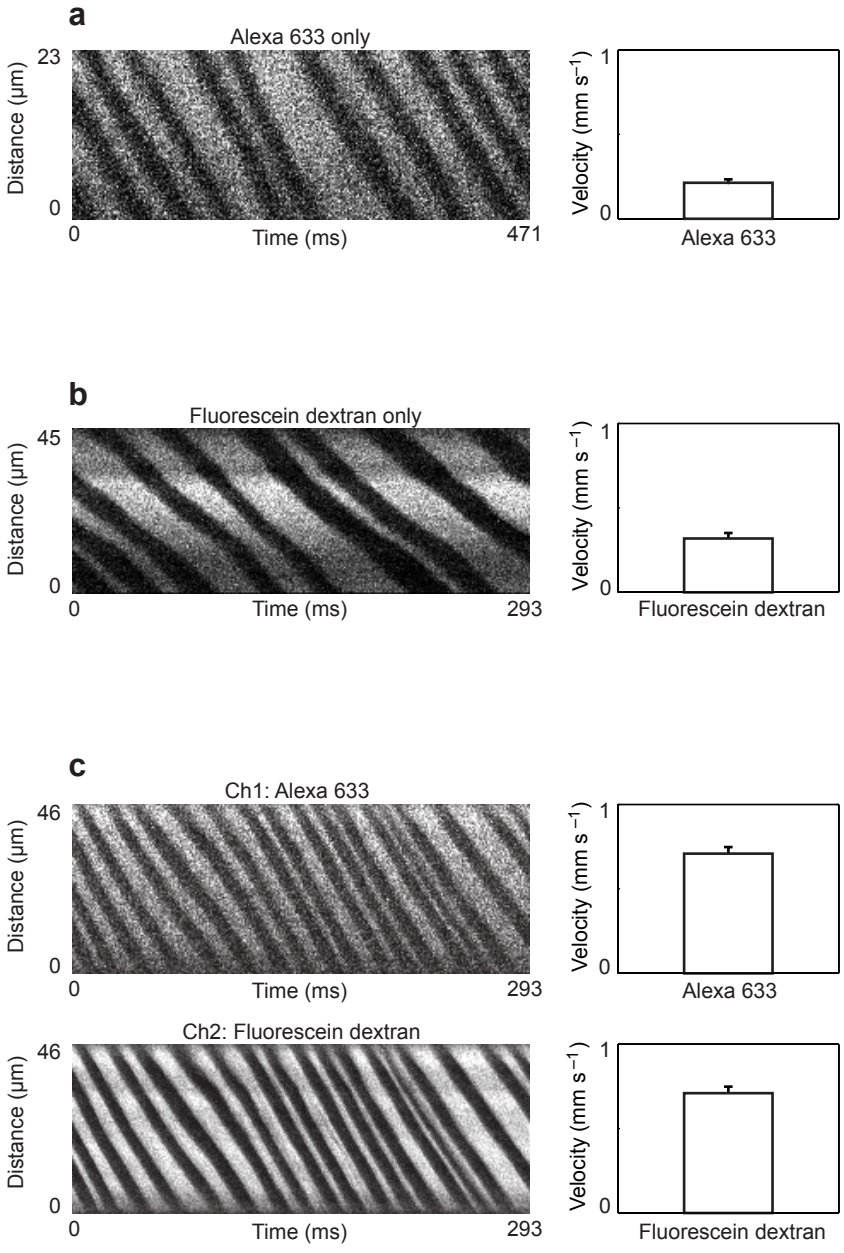

Supplementary Figure 19
Red blood cell velocity in cortical microvessels after intravenous injection of fluorescent dyes

(**a**) Rat 1. Red blood cell velocity from line scans after an intravenous injection of Alexa 633. No fluorescein dextran was injected in this rat. Line scans were collected before Alexa 633 cleared the blood plasma.

(**b**) Rat 2. Red blood cell velocity from line scans after intravenous injection of fluorescein dextran. No Alexa 633 was injected in this rat.

(**c**) Rat 3. Red blood cell velocity from line scans after intravenous injection of Alexa 633 (recorded on PMT Channel 1) and fluorescein dextran (recorded on PMT Channel 2). Cross talk between the two PMT channels was eliminated by careful selection of PMT gain and the wide separation of emission bands between the red and green PMT filters used for Alexa 633 and fluorescein dextran imaging. As expected, line scan imaging on Alexa 633 and fluorescein dextran channels resulted in virtually identical mean velocity measurements.

Raw line scan data shown for each of the three rat experiments are from a block of 200 line scans. In the mean velocity plots (right panels) error bars are standard deviations.

Supplementary Figure 20
Light path used for *in vivo* two-photon imaging

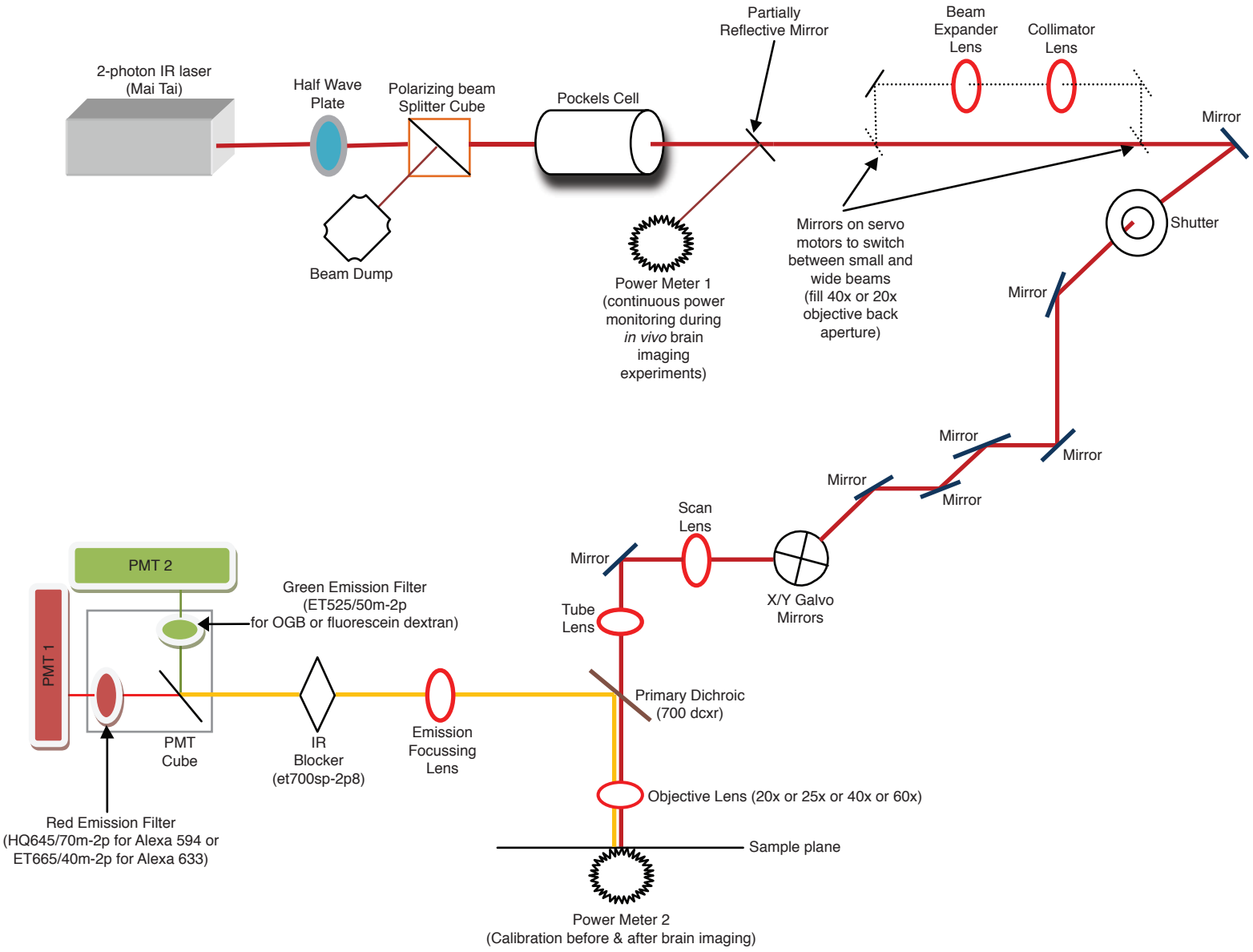

Supplementary Figure 20
Light path used for *in vivo* two-photon imaging

Note that the specifications for objective lenses and a detailed protocol for line & frame scans are provided in the Methods.

Supplementary Note 1

Fluorescence dip artifact caused by arteriole dilation

Guided by Alexa 633, we showed that arteriole dilation acts like a stimulus-evoked filter and leads to stimulus-evoked dips in fluorescence from neurons located directly under arterioles but not veins. We suggest that claims in the literature of the presence of reductions in neural spiking activity (relative to spontaneous baseline firing) from calcium indicator imaging should also include the location of these neurons relative to surface arterioles. Also, the reports should explicitly demonstrate that arteriole dilation is not the source of decreases in neuronal fluorescence. Measurements of neuronal tuning bandwidth inferred from calcium indicator imaging also should include careful consideration of surface arteriole locations. The exact mechanism of how two-photon light passage through the dilating arteriole leads to a reduction in neuronal fluorescence remains to be determined. Perhaps, compared to the unstimulated baseline period, the relatively rapid dilation of arterioles upon sensory visual stimulation produces a larger local hemoglobin volume. This increased volume of hemoglobin absorbs more two-photon excitation light and emitted fluorescence from neurons. However, light scattering from the complex architecture of the arterial wall including the molecular dynamics of elastin fibers[23] should not be ruled out.

Supplementary Note 2

Selectivity of Alexa 633 vs. other rhodamine derivatives

Alexa 633 is a sulfonated rhodamine derivative[24]. Different rhodamine derivatives have been reported to have selectivity for various cell types. Rhodamine-6G labels leukocytes[25]. Rhodamine-123 labels mitochondria[26]. Sulforhodamine-101 and sulforhodamine-B label astrocytes[27,28]. Astrocyte-selective markers like sulforhodamine-101 and sulforhodamine-B will, by definition, outline many vessels including capillaries in the brain via astrocyte end-feet apposition to blood vessels[27]. More recently, sulforhodamine-101 has been suggested to also label endothelial cells lining arteries in the cerebral cortex[29], but such labeling of multiple cell classes with sulforhodamine-101 means that distinguishing arterioles from venules remains difficult. The labeling of different cell types alongside vessels of different classes also makes it difficult to use sulforhodamine-101 to track changes in vessel diameter. Finally, sulforhodamine-101 via astrocyte labeling has been reported to induce epileptic seizures by lowering the neuronal action potential threshold[30], further undermining the use of this compound in neurovascular coupling studies *in vivo*. Our methods provide strong evidence for artery and arteriole specificity of Alexa 633 in the brain—bright labeling of a continuous band of elastin fibers wedged between smooth muscle and endothelial basement membrane (with no labeling of neurons, astrocytes, veins, venules, or pericytes). It is possible that excessively high concentrations of Alexa 633 application—via many dozens of high pressure pulses through the micropipette rather than just a few low

pressure pulses of a few psi, or higher than our suggested intravenous dose, combined use of detergents like DMSO, or any stress (e.g., physical, chemical, oxidative, metabolic), that induces astrocytes to become reactive may all lead to non-specific labeling. Poor PMT filter design and resulting cross talk from OGB or GFP labeled neurons and/or astrocytes may also lead to the appearance of non-specific labeling. Although we have examined labeling in five tissue types across five species, we cannot exclude the possibility that some veins in other species or tissues may also take up Alexa 633. Possibly, some peripheral vasculature in the extremities of the limbs, large veins like the superior vena cava in some species, or parenchymal cells in the liver could take up Alexa 633. For example, we have observed some dis-continuous Alexa 633 labeling in femoral veins (data not shown). Note that the astrocyte-specific dye sulforhodamine-101 (discussed above) also labels oligodendrocytes in the retina[31] and motor neurons that innervate peripheral muscles[32]. Our review of the literature on the anatomy of veins and venules throughout the body suggest that the presence of a continuous band of elastin in these structures is rather unlikely. But regardless of any future uncovering of accumulation of Alexa 633 in cells or connective tissue in some part of the body, our study establishes the utility for Alexa 633 in neurovascular coupling research.

Supplementary References

23. Tamburro, A.M. *Nanomedicine (Lond.)* **4**, 469-487 (2009).

24. Agnew, B., Gee, K.R. & Nyberg, T.G., United States Patent Application No. 0249014 (Oct. 25, 2007).

25. Schwarzmaier, S.M., Kim, S.W., Trabold, R. & Plesnila, N. *J. Neurotrauma* **27**, 121-130 (2010).

26. Johnson, L.V., Walsh, M.L. & Chen, L.B. *Proc. Natl. Acad. Sci. USA* **77**, 990-994 (1980).

27. Nimmerjahn, A., Kirchhoff, F., Kerr, J.N. & Helmchen, F. *Nat. Methods* **1**, 31-37 (2004).

28. Verant, P., Ricard, C., Serduc, R., Vial, J.C. & van der Sanden, B. *J. Biomed. Opt.* **13**, 064028 (2008).

29. McCaslin, A.F., Chen, B.R., Radosevich, A.J., Cauli, B. & Hillman, E.M. *J. Cereb. Blood Flow Metab.* **31**, 795-806 (2011).

30. Kang, J. *et al. Neuroscience* **169**, 1601-1609 (2010).

31. Ehinger, B., Zucker, C.L., Bruun, A. & Adolph, A. *Glia* **10**, 40-48 (1994).

32. Lichtman, J.W., Wilkinson, R.S. & Rich, M.M. *Nature* **314**, 357-359 (1985).